Fabrication of corrugated artificial insect wings using laser micromachined molds

2010 J. Micromech. Microeng. 20 075008

(http://iopscience.iop.org/0960-1317/20/7/075008)

J. Micromech. Microeng. **20** (2010) 075008 (8pp) doi:10.1088/0960-1317/20/7/075008

Fabrication of corrugated artificial insect wings using laser micromachined molds

Hiroto Tanaka and Robert J Wood

School of Engineering and Applied Sciences, Harvard University, 60 Oxford Street, Cambridge, MA 02138, USA

E-mail: rjwood@seas.harvard.edu

Received 9 March 2010, in final form 6 April 2010
Published 21 May 2010
Online at stacks.iop.org/JMM/20/075008

Abstract

This paper describes the fabrication of an artificial insect wing with a rich set of topological features by micromolding a thermosetting resin. An example 12 mm long hoverfly-like wing is fabricated with 50–125 μm vein heights and 100 μm corrugation heights. The solid veins and membrane were simultaneously formed and integrated by a single molding process. Employing a layered laser ablation technique, three-dimensional molds were created with 5 μm resolution in height. Safe demolding of the wing was achieved with a water-soluble sacrificial layer on the mold. Measured surface profiles of the wing matched those of the molds, demonstrating the high replication accuracy of this molding process. Using this process, the morphological features of insect wings can be replicated at-scale with high precision, enabling parametric experiments of the functional morphology of insect wings. This fabrication capability also makes it possible to create a variety of wing types for micro air vehicles on scales similar to insects.

(Some figures in this article are in colour only in the electronic version)

1. Introduction

The aerodynamic performance of flying insects is highly dependent on the morphology of the wings. Since insects do not have muscles distal to the wing base (unlike birds and bats), any deformation of the wings during flight is solely due to the inertial and aerodynamic loads coupled to the wing structure [1–6]. Insect wings consist of thin membranes supported by a network of tubular veins [7]. Additionally, some parts of the wing surface exhibit a three-dimensional (3D) corrugated profile. The combination of veins and corrugation allows the wing to deform in various prescribed ways when subject to different loading conditions [8–11]. Such deformations can range from simple linear elastic bending modes to buckling instabilities. Beyond structural significance, the corrugated wing profile also is thought to play a role in lift and drag coefficients for low Reynolds number conditions [12–14]. The magnitude of the effect of these vein and corrugation structures in actual flapping flight, however, is still unknown. One of the reasons is a lack of parametric experiments of natural insect wings. Previous studies on flapping-wing designs have typically used large-scale models [15–17]. However, in such cases, inertial and viscous forces scale in a fundamentally different manner from elastic forces, and therefore, such studies are not able to decipher the contributions of morphological features to aeroelastic performance benefits. Several fabrication methods for small biomimetic wings have been proposed, primarily for use in the development of micro air vehicles (MAVs) [18–25]. However, an insect-scale wing which can recreate the veins and corrugations of natural wings has never been achieved due to the difficulty of integrating different 3D micro-scale features: veins, corrugation and the membrane.

In this paper, we describe the fabrication of an artificial insect wing having veins and corrugations by micromolding a thermosetting resin. The veins and membrane were formed and integrated by a single molding process with 3D molds. To create the 3D shape of the molds, we employed a layered laser machining technique. Various metal and polymer materials can be machined by laser ablation, and micro-scale 3D structures created by laser ablation were previously reported [26–33]. Using laser scanning ablation, arbitrary 3D shapes can be created subject to the resolution of the scanner and the laser spot size and quality. With this process, the surface profiles of veins and corrugations of natural insect wings can be reconstructed in the artificial wings at the same scale using

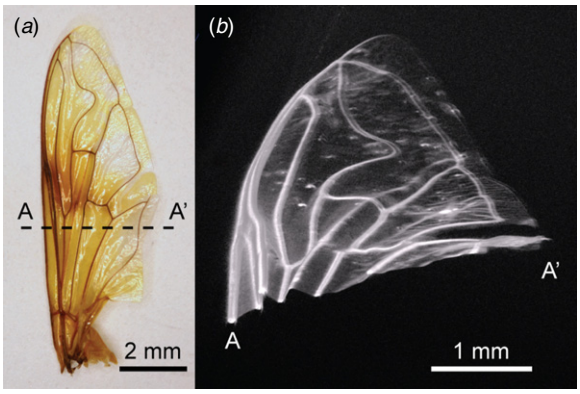

Figure 1. Wing of the hoverfly, *E. tenax*. (*a*) Dorsal side of the wing surface. (*b*) Corrugated section captured by 3D x-ray CT. The wing was stained with iodine for the x-ray CT.

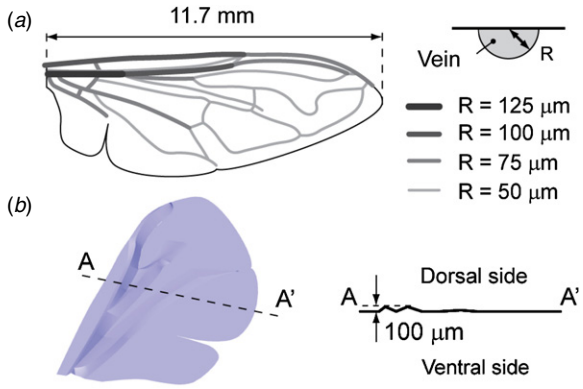

Figure 2. Design of the artificial fly wing. (*a*) Planar shape and vein pattern. The wing has four different thicknesses of veins on the ventral surface. (*b*) 3D model for corrugation. Maximum height of corrugation is 100 μm.

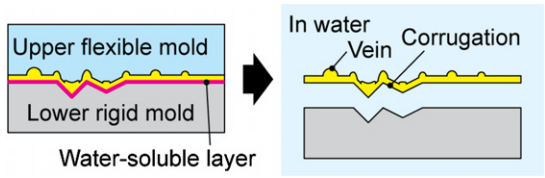

Figure 3. Concept sketch of the molding of 3D wing with veins and corrugation. Liquid resin is sandwiched between upper and lower molds. A water-soluble sacrificial layer on the lower mold enables the cured wing to be demolded without physical or chemical damage.

materials with similar elastic properties as those found in natural insect wings (e.g. 1–20 GPa [34–37]). In addition, once the molds are made, the wings can be replicated with high precision with minimal effort.

Our artificial wing enables parametric experiments on the functional morphology of insect wings with insect-scale models. We can design, fabricate and compare different types of veins and corrugations. This fabrication capability is also useful for the development of MAVs. A variety of wings can be designed and replicated according to the requirement of the MAV. In this paper, we describe the fabrication of an artificial hoverfly wing as an example of a veined and corrugated wing. Details of the fabrication process and quantifications of the resulting structures are described in following sections.

2. Materials and methods

2.1. Fabrication

To begin, we chose to base our designs on a hoverfly, *Eristalis tenax* (figure 1(*a*)). This species was chosen since the wings of *Eristalis* (as well as other Diptera) exhibit a rich topology including veins of multiple sizes and corrugation patterns [8]. The wing length of *E. tenax* was 11 mm and the vein thicknesses ranged from 8 to 70 μm. To more fully understand the topology of the wing, we generated a 3D representation of the wing using x-ray microtomography (CT) (figure 1(*b*)). There are two deep corrugations near the leading edge with heights approximately 150 μm from peak to peak. We then translated these key features into a CAD model (figure 2). The planar shape and vein pattern were obtained by tracing those of the real wing (figure 2(*a*)). The veins have solid semicircular cross sections with four different radii; 125, 100, 75 and 50 μm. The maximum corrugation height is 100 μm. For ease of fabrication, the vein widths are larger than those of the real wing and corrugation height is smaller. The veins are only on the ventral surface for the same reason. Nevertheless, the dimensions of the artificial and real wings are comparable.

The basic idea of our fabrication method for the 3D wing is compression molding with 3D molds (figure 3). By sandwiching a liquid resin between lower and upper molds, veins integrated with a corrugated membrane can be obtained. A water-soluble sacrificial layer [38] on the lower mold enables demolding of the wing from the complex mold without physical or chemical damage. There are three advantages of this method. First, veins are assembled without manual manipulation. This reduces both physical variations and fabrication time. Second, veins are integrated with the membrane without extra bonding processes. This prevents any unnecessary increase in wing mass due to excess adhesive or adhesion failure at vein–membrane interfaces. Third, arbitrary 3D shapes of veins and corrugation can be obtained according to the manufacturability of the 3D molds. Additionally, the use of polymers for the wing materials affords resilience to potential failure during use. Moreover, the modulus of available polymers is similar to that of insect wing veins [34–37].

To realize this method, and considering the feature sizes of insect wings, it is necessary to create the 3D molds with less than 10 μm resolution in both thickness and planar directions. We used a custom-made diode-pumped solid-state (DPSS) laser machining system as a mold-making tool. The laser (Nd: YVO4) has a 355 nm wavelength and can cut materials which absorb 355 nm radiation by ablation (e.g. most metals, ceramics and semiconductors). The maximum average power was approximately 2 W and the pulse duration was 15 ns with a 20 kHz pulse repetition rate. The spot size of the laser was nominally 10 μm. The scan speed was adjusted so that the laser spots lined up without gaps to ensure a maximally smooth

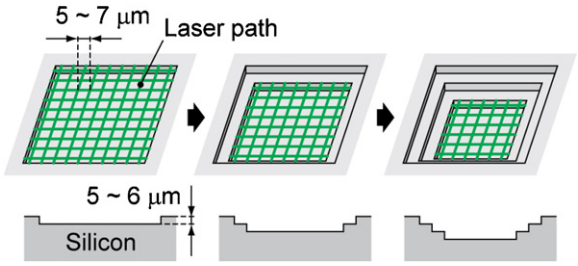

Figure 4. Schematic of laser etching of the 3D mold. The silicon wafer was etched by orthogonal scanning of a diode-pumped solid-state (DPSS) laser across the surface of a silicon wafer. Layer-by-layer etching creates a user-defined 3D shape.

ablated surface. For a 20 kHz pulse repetition rate, the scan speed was 200 mm s^{-1}. Figure 4 shows a schematic of the laser machining process of the 3D mold. The mold surface is etched by laser scanning in orthogonal directions. We can create arbitrary 3D shapes by changing the scanning area for each etching layer. The spacing between laser paths, scan speed and laser energy was tuned for the desired etching rate and surface quality. Silicon was chosen as the mold material primarily due to its applicability to ablation at 355 nm. To verify and calibrate the etching process, we fabricated three types of 200 μm wide channels having rectangular, triangular and semi-circular cross sections, respectively (figures 5(*a*)–(*f*)). The spacing of the laser path was set to 5 μm with a total of 20 etching layers. The targeted etching rate was 5 μm per layer for a 100 μm channel depth. As a result, a 5 μm etching rate was achieved for each channel. In the rectangular-section channel, the walls of the channel were not vertical since the laser ablation process is fundamentally an aspect-ratio-limited process (figure 5(*b*)). However, the semi-circular and triangular sections matched the desired profile (figures 5(*d*), (*f*)).

The detailed fabrication process for the artificial insect wing is depicted in figure 6. A lower silicon mold with corrugation was fabricated by layered laser machining (figure 6(1)). The planform design for each etching layer was generated by slicing a 3D model of the wing using 3D CAD software (Rhinoceros, Robert McNeel & Associates). The targeted etching rate was 6 μm per layer and the spacing of the laser path was set at 7 μm. Since the designed maximum corrugation height was 100 μm, we required 16 etching layers. Alignment holes (250 μm deep) were also created simultaneously. These holes were used to align the upper and lower molds in the molding process. A flexible upper mold was made by casting polydimethylsiloxane (PDMS) (Sylgard 184, Dow Corning, 10:1 mixing weight ratio of base to curing agent) on a second silicon mold. Fabrication of this mold begins by creating convex vein patterns on a silicon wafer using the same layered laser machining process described above (figure 6(2)). The designed maximum height of the veins was 125 μm, requiring 21 etching layers. Following formation of the veins, a concave corrugation pattern was laser machined on the vein pattern using the same CAD data as the lower mold (figure 6(3)). That is, the resultant shape was the sum of the convex veins and concave corrugation. Alignment holes

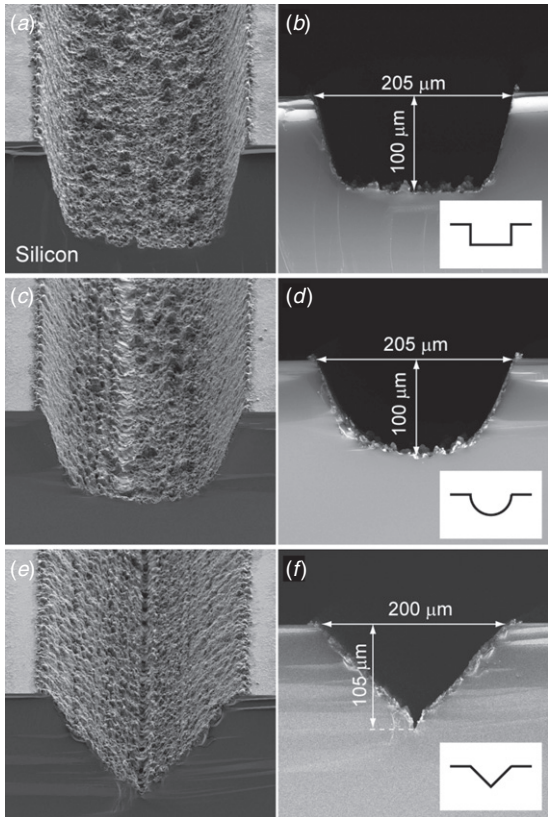

Figure 5. SEM images of laser-etched silicon channels. Rectangular-section (*a*), (*b*), semicircular-section (*c*), (*d*) and triangular-section channels (*e*), (*f*) were created by 20 layers of laser etching.

(180 μm deep) for the PDMS mold and 20 μm thick holes for spacers for the wing membrane were also created in this step. This silicon machining step creates a positive mold which will be used to create the compliant negative upper mold. The surface of the silicon mold was rendered hydrophilic with an oxygen plasma treatment (30 s, 100 W, 30 cc min^{-1}, 320 mTorr; Plasma Prep III, SPI Supplies/Structure Probe Inc.). Then a water-soluble sacrificial layer was deposited on the silicon mold surface as a release agent by spin-coating a 7% poly(acrylic acid) (PAA) solution (neutralized with a 4% sodium hydroxide solution) at 1000 rpm for 15 s and baking on a hotplate at 150 °C for 2 min (figure 6(4)). PDMS was cast on the silicon mold, degassed in a vacuum for 1 h and cured at room temperature for 24 h. The cured upper PDMS mold was peeled from the silicon mold in water (figure 6(5)). The surface of the upper PDMS mold was silanized with trichloro(1H, 1H, 2H, 2H-perfluorooctyl)silane to assist demolding of the final wing during the molding process described below.

The wing molding process begins by spin-coating PAA on the lower mold (figure 6(6)). Next, a thermosetting resin (Tuffalloy4282, Hapco Inc.) was cast on the upper mold in a vacuum chamber (figure 6(7)). According to the datasheet of the resin, its viscosity is 270 cps, gel time is 7 min and the flexural modulus (post cure) is 3.2 GPa. This resin was chosen for its high flexural modulus and ease of casting and curing. It is possible to use different thermosetting resins as well as additives (e.g. milled or chopped fibers) to

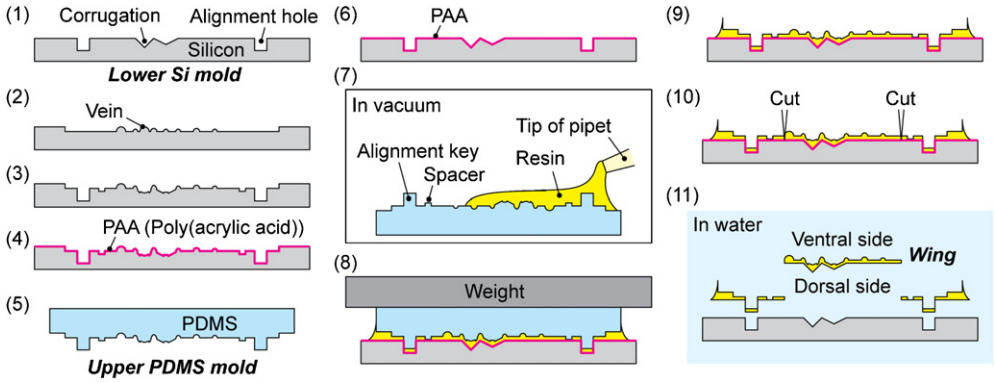

Figure 6. Process flow for wing molding. (1)–(3) Silicon molds were fabricated by laser machining. (4), (5) The upper mold was made by casting PDMS onto the laser-machined silicon positive mold assisted with a PAA release layer. (6)–(8) The 3D wing was molded with the upper and lower molds. (9), (10) After the wing was cured, the upper mold was removed and the wing outline was cut with a laser. (11) The 3D wing was demolded in water without physical or chemical damage.

modify the mechanical property of the wing. After the resin covered the surface of the mold, the upper mold was taken out of the vacuum chamber, flipped upside-down, and placed on the lower mold (figure 6(8)). The upper mold was physically aligned with the lower mold by the alignment keys and holes and the wing was cured for 2 h at room temperature. The upper mold was manually peeled off after the initial cure (figure 6(9)). The wing was then baked at 75 °C for 12 h for a full cure. After cutting an outline of the wing with a laser (figure 6(10)), the lower mold with the wing was soaked in a water for several hours (figure 6(11)). Most parts of the wing were separated from the lower mold without manual manipulation. Any remaining portions adhering to the mold were manually released.

2.2. *Characterization*

To quantify the topology of the fabricated wing, we measured the surface profiles of the wing and the original silicon molds with a laser scanning confocal microscope (LEXT OLS4000, Olympus Corp.). We also compared the morphological parameters of the artificial wing with those of a natural fly, *E. tenax*. The membrane thicknesses and vein radii of the natural wing were measured with a microscope after cutting the wing with a scalpel at the same section line as the profile measurement of the artificial wing. Wing mass was measured with a precise automatic electrobalance (Cahn 25, Cahn/Ventron)

To characterize the static properties of the artificial wing, we measured the flexural stiffnesses of both the artificial and natural wings by applying a point force to bend the wings. The overall flexural stiffness EI was approximated from the applied force and the displacement of the wing using simple beam theory, where E is Young's modulus of the beam and I is the second moment of area of the cross section. A schematic of the measurement setup is shown in figure 7. We used a dead specimen of *E. dimidiata*, which has a similar wing shape and size to *E. tenax*, for comparison due to the availability of the fly specimen. The wings were glued to 1.0 × 25 × 75 mm glass slides with a cyanoacrylate glue at the wing base. The glass slides were clamped onto the z-axis slider with a micrometer

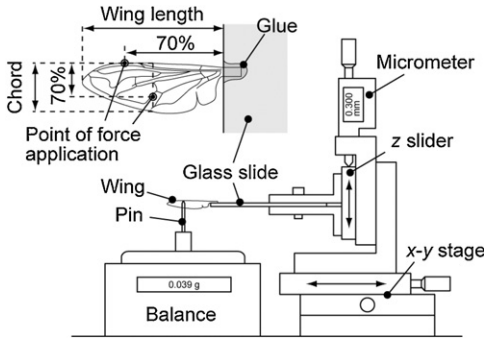

Figure 7. Schematic of the flexural stiffness measurement. Left upper: for spanwise measurements, point forces were applied at approximately 70% of the wing length on the leading edge. For chordwise measurements, point forces were applied at 70% of the chord width at half the wing length. Bottom: the applied force was measured with a balance, and deflection of the wing was measured with a micrometer.

mounted on an x–y linear stage. The wing was lowered until it contacted a rounded-tip pin placed on a balance. By lowering the wing further, a point force was applied to the wing. The applied force and the displacement of the wing were measured with the balance and the micrometer, respectively. To ensure the initial contact, we reset the balance and the micrometer as zero when the applied force reached 10 mg. The flexural stiffness was calculated as

$$EI = fl^3/3\delta \tag{1}$$

where f is the applied force, l is the distance between the point of force application and the proximal mount, and δ is the displacement of the wing at the point of force application [39]. We applied the point force from the ventral side at approximately 70% of the wing length on the leading edge for the spanwise stiffness and at 70% of the chord width at half the wing length for the chordwise stiffness. These positions were chosen to be consistent with the previous stiffness measurements of insect wings executed by Combes and Daniel [1]. For the calculation of spanwise stiffness, we used the distance between the edge of the glass slide and the point of force application as l. For chordwise stiffness, we

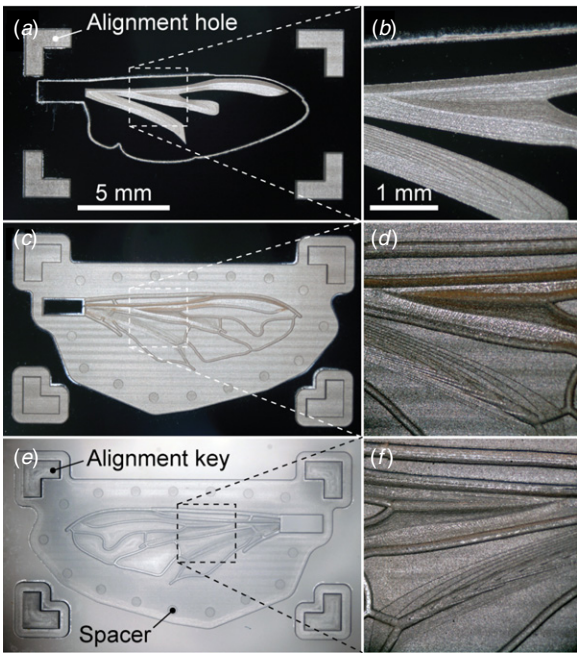

Figure 8. Photos of fabricated molds. Lower silicon mold with concave corrugations (*a*), (*b*). Silicon mold for the upper PDMS mold has convex veins and concave corrugations (*c*), (*d*). The upper PDMS mold has concave veins and convex corrugations (*e*), (*f*).

used the distance between the leading edge and the point of force application as l, assuming a small bending deformation of the leading edge. The displacement d was ensured to be smaller than 5% of l since equation (1) is only applicable for small deflections.

To verify our method for measuring reduced stiffness, we estimated the flexural modulus E of a thin rectangular cover glass (0.155 × 24 × 60 mm) from the measured EI and compared it with the known value for a cover glass. The cover glass was glued to the glass slide as described above. The point force was applied at a distance of 53 mm. For a rectangular cross section, the second moment of area I was expressed as

$$I = wt^3/12 \tag{2}$$

where w is the width and t is the thickness. From the measured EI and the calculated I, Young's modulus E was estimated. The displacement was varied from 100 to 1000 μm and the estimated E ranged from 6.9 to 6.6 × 10^{10} Nm^{-2}, which are in good agreement with the known value of 6.9 × 10^{10} Nm^{-2} [39], validating this method for static estimations of the reduced flexural stiffness.

3. Results and discussion

The laser-machined molds are shown in figure 8. Two deep corrugations at the leading edge and a small corrugation at the center of the wing were created on a lower silicon mold (figure 8(*a*)). Though the quantized steps from laser machining are apparent on the gentle slopes, steep slopes and the curved shape of veins were smooth (figures 8(*b*), (*d*)). The shapes of the silicon mold were transferred to a PDMS upper mold without any voids or damage (figures 8(*e*), (*f*)). The

Figure 9. Fabricated artificial fly wing on a finger.

20 μm thick circular spacers are intended to control the wing membrane thickness and are arranged around the wing pattern on the upper PDMS mold (figure 8(*e*)). Alignment holes and keys at the four corners fixed the position and orientation of the upper PDMS mold to the lower silicon molds, eliminating the need for manual alignment tools and techniques (figures 8(*a*), (*e*)). Alignment holes were also used as marks for the final laser cutting of the wing outline after molding. The trace of the outline cutting on the lower silicon mold can be seen in figure 8(*a*). A rectangular handle was also fabricated at the wing base (figures 8(*c*), (*e*)).

The final 3D artificial insect wing and its surface profiles are shown in figures 9 and 10. On the dorsal surface, there are convex corrugations without veins (figures 10(*a*), (*b*)). The veins were molded on the ventral surface without any voids (figures 10(*c*), (*d*)). The vein pattern which was seen through the wing from the dorsal side showed that the veins on the ventral side and corrugations on the dorsal side were accurately aligned (figures 10(*a*), (*b*)). To verify the accuracy of the shape transfer of the molding, we measured the surface profiles of the wing and silicon molds with the laser scanning confocal microscope. The measured profile of the dorsal surface shows two deep corrugations (figure 10(*e*)) as designed in figure 2(*b*). The profile of the ventral surface was the sum of the convex venation and the concave corrugation as explained in section 2 (figures 6(2), (3)). The wing profiles matched with those of the original silicon molds (figure 10(*f*)), demonstrating the accuracy of the replication method. Furthermore, any discrepancies between the actual insect wing and the molded wing are purely due to design as opposed to molding or alignment errors.

The key morphological parameters of both the artificial and natural wings are given in table 1. The wing length of the artificial wing was 11.7 mm with a mass of 1.42 mg (without the handle). The veins have solid semicircular cross sections and their radii were 50, 75, 100, 125 μm as designed in figure 2(*a*). The measured membrane thicknesses ranged from 10 to 20 μm. Compared with a natural wing, the wing length was similar to that of a natural wing, but the wing mass (1.42 mg) was greater than that of a natural wing (0.53 mg) (table 1). This is assumed to be due to the thicker artificial membrane and veins. Additionally, the artificial veins have

Table 1. Morphological parameters of artificial and natural wings.

	Wing length (mm)	Vein thickness (μm)	Membrane thickness (μm)	Corrugation height (μm)	Wing mass (mg)
Artificial wing	11.7	50, 75, 100, 125	10 to 20	100	1.42
E. tenax	11.4[a]	8 to 70	1 to 3	150	0.53[a]

[a] Taken from [40] for a fresh specimen.

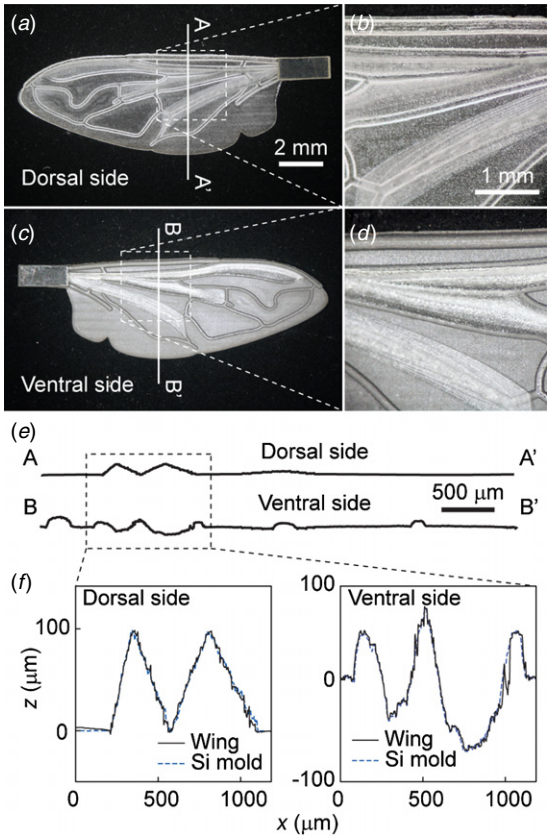

Figure 10. Surface profiles of fabricated wing and silicon molds. The dorsal surface of the wing had convex corrugations (*a*), (*b*). The ventral surface had concave corrugations and convex veins (*c*), (*d*). The measured profiles showed polygonal corrugation and semicircular vein cross sections (*e*). The profiles of the wing matched those of the original silicon molds (*f*).

solid cross sections, while insect veins have tubular cross sections [7, 8]. A hollow cross section is an ideal design for maximizing stiffness with minimal mass. The second moment of area I of a hollow tube is expressed as

$$I = \frac{\pi}{4}\left(r_1^4 - r_2^4\right) \tag{3}$$

where r_1 is an external radius and r_2 is an internal radius [39]. Assuming a tube of $r_1 = 2r_2$, the resultant I would be 94% of that of the solid cylinder with the same external radius, while the mass of the tube, which is proportional to the cross-sectional area, would be 75% of that of the solid cylinder.

Tubular veins are impossible to fabricate by the current method, but cross-sectional shapes can be arbitrarily adjusted (to the limits of the wall slopes described in section 2.1). For example, high-aspect-ratio U-shape or rectangular sections are possible alternatives to the present low-aspect-ratio semicircular sections for reduced vein mass and/or increased stiffness. Since the second moment of area of the rectangular section is proportional to the cube of the thickness as shown in equation (2), the flexural stiffness of the veins can be drastically increased with the vein height rather than width. High-aspect-ratio structures, however, tend to make it difficult to safely remove the upper PDMS mold. In that case, additional processes for demolding (e.g. smoothing the mold surface) may be required. The membrane thickness can be decreased by reducing the spacer height of the upper mold. The minimum spacer height is 6 μm, which is determined by the step height of the layered laser machining of the mold. By eliminating the spacers, the membrane thickness can be reduced further and controlled with the pressure applied to the mold during the molding process.

Table 2. Flexural stiffness of the artificial and natural wings.

	Wing length (mm)	Spanwise EI (N m^{-2})	Chordwise EI (N m^{-2})
Artificial wing	11.7	2.2×10^{-7}	2.1×10^{-8}
E. dimidiata	9.3	5.3×10^{-7}	2.4×10^{-9}

The measured spanwise flexural stiffness of the artificial wing (2.2×10^{-7} N m^{-2}) was smaller than that of a natural wing (5.3×10^{-7} N m^{-2}) despite the thicker solid artificial veins (table 2). This is assumed to be due to the smaller corrugation of the artificial wing (table 1). As for the material properties of the natural wing, it is possible that the leading edge of the natural wing had a higher Young's modulus than other areas [34]. Furthermore, it has been observed that dry wings are stiffer than fresh wings [41]. In contrast to the spanwise flexural stiffness, the chordwise flexural stiffness of the artificial wing (2.1×10^{-8} N m^{-2}) was higher than that of the natural wing (2.4×10^{-9} Nm^{-2}). This is primarily due to the difference between membrane thicknesses of the artificial and natural wings (table 1). One potential remedy to these discrepancies involves employing high-aspect-ratio sections for the leading edge veins and decreased membrane thickness as described before.

It should be noted that the measured stiffness of *Eristalis* in this paper was smaller than those reported by Combes and Daniel [1] by an order of magnitude for the spanwise direction and two orders of magnitude for the chordwise direction even though our wing was not fresh. Since both measurement setups were verified with a cover glass and the locations of force application were similar, the difference was thought to derive from the attachment methods of the wings and the shapes of the tips of the pins for force application.

4. Conclusion

We have demonstrated a micromolding method for a corrugated artificial insect wing. The wing, which was made of a thermosetting resin, contains veins on a corrugated membrane mimicking the morphological features of a natural hoverfly. The veins and membrane were simultaneously formed and integrated by a single molding process with three-dimensional molds. The three-dimensional surfaces of the molds were created by layered UV-laser micromachining. An etch rate of 5 μm per layer was achieved for silicon by appropriately tuning the laser settings. A spin-coated water-soluble sacrificial layer was utilized to assist demolding. This layer enabled the fragile thin wing to be demolded from the complex 3D mold without physical or chemical damage. Using this method, we fabricated an artificial fly wing having a 100 μm height corrugation and 50 to 125 μm radius semicircular veins. The surface profiles of the fabricated wing matched those of the original molds, indicating an accuracy of replication. The measured spanwise stiffness of the fabricated wing was 2.2×10^{-7} Nm^{-2}, which is the same order of magnitude as that of a natural wing.

Our method makes it possible to fabricate and replicate insect-sized wings having arbitrary 3D shape with micron-order precision. This has the potential to expand the design space for MAV airfoils. Artificial insect wings will also be useful for experimental research on the functional morphology of insect flight. Using insect-sized artificial wings, design parameters can be precisely controlled and compared without the need to consider scale effects.

Acknowledgments

The authors gratefully acknowledge support from the National Science Foundation (award number CCF-0926148). Any opinions, findings and conclusions or recommendations expressed in this material are those of the authors and do not necessarily reflect those of the National Science Foundation. The authors also acknowledge support of the Wyss Institute for Biologically Inspired Engineering and the facilities in the Harvard Center for Nanoscale Systems. The authors thank Peter Whitney for discussions on laser machining.

References

[1] Combes S A and Daniel T L 2003 Flexural stiffness in insect wings: I. Scaling and the influence of wing venation *J. Exp. Biol.* **206** 2979–87

[2] Combes S A and Daniel T L 2003 Flexural stiffness in insect wings: II. Spatial distribution and dynamic wing bending *J. Exp. Biol.* **206** 2989–97

[3] Ennos A R 1988 The importance of torsion in the design of insect wings *J. Exp. Biol.* **140** 137–60

[4] Ennos A R 1988 The inertial cause of wing rotation in Diptera *J. Exp. Biol.* **140** 161–9

[5] Ennos A R 1989 Inertial and aerodynamic torques on the wings of Diptera in flight *J. Exp. Biol.* **142** 87–95

[6] Young J, Walker S M, Bomphrey R J, Taylor G K and Thomas A L R 2009 Details of insect wing design and deformation enhance aerodynamic function and flight efficiency *Science* **325** 1549–52

[7] Wootton R J 1992 Functional-morphology of insect wings *Annu. Rev. Entomol.* **37** 113–40

[8] Rees C J C 1975 Form and function in corrugated insect wings *Nature* **256** 200–3

[9] Wootton R J 1993 Leading edge section and asymmetric twisting in the wings of flying butterflies (Insecta, Papilionoidea) *J. Exp. Biol.* **180** 105–17

[10] Wootton R J and Ennos A R 1989 The implications of function on the origin and homologies of the dipterous wing *Syst. Entomol.* **14** 507–20

[11] Wootton R J, Herbert R C, Young P G and Evans K E 2003 Approaches to the structural modelling of insect wings *Philos. Trans. R. Soc.* B **358** 1577–87

[12] Kesel A B 2000 Aerodynamic characteristics of dragonfly wing sections compared with technical aerofoils *J. Exp. Biol.* **203** 3125–35

[13] Okamoto M, Yasuda K and Azuma A 1996 Aerodynamic characteristics of the wings and body of a dragonfly *J. Exp. Biol.* **199** 281–94

[14] Sunada S, Yasuda T, Yasuda K and Kawachi K 2002 Comparison of wing characteristics at an ultralow Reynolds number *J. Aircr.* **39** 331–8

[15] Birch J M and Dickinson M H 2001 Spanwise flow and the attachment of the leading-edge vortex on insect wings *Nature* **412** 729–33

[16] Dickinson M H, Lehmann F O and Sane S P 1999 Wing rotation and the aerodynamic basis of insect flight *Science* **284** 1954–60

[17] Lu Y and Shen G X 2008 Three-dimensional flow structures and evolution of the leading-edge vortices on a flapping wing *J. Exp. Biol.* **211** 1221–30

[18] Shang J K, Combes S A, Finio B M and Wood R J 2009 Artificial insect wings of diverse morphology for flapping-wing micro air vehicles *Bioinspir. Biomim.* **4** 036002

[19] Madangopal R, Khan Z A and Agrawal S K 2005 Biologically inspired design of small flapping wing air vehicles using four-bar mechanisms and quasi-steady aerodynamics *J. Mech. Des.* **127** 809–16

[20] Tanaka H, Matsumoto K and Shimoyama I 2008 Design and performance of micromolded plastic butterfly wings on butterfly ornithopter *IROS 2008: 2008 IEEE/RSJ Int. Conf. on Intelligent Robots and Systems* pp 3095–100

[21] Fujikawa T, Hirakawa K, Okuma S, Udagawa T, Nakano S and Kikuchi K 2008 Development of a small flapping robot: motion analysis during takeoff by numerical simulation and experiment *Mech. Syst. Signal Proc.* **22** 1304–15

[22] Tanaka H, Matsumoto K and Shimoyama I 2007 Fabrication of a three-dimensional insect-wing model by micromolding of thermosetting resin with a thin elastmeric mold *J. Micromech. Microeng.* **17** 2485–90

[23] Wood R J 2008 The first takeoff of a biologically inspired at-scale robotic insect *IEEE Trans. Robot.* **24** 341–7

[24] Dargent T, Bao X Q, Grondel S, Brun G L, Paquet J B, Soyer C and Cattan E 2009 Micromachining of an SU-8 flapping-wing flying micro-electro-mechanical system *J. Micromech. Microeng.* **19** 085028

[25] Pornsin-sirirak T N, Tai Y C, Nassef H and Ho C M 2001 Titanium-alloy MEMS wing technology for a micro aerial vehicle application *Sensors Actuators* A **89** 95–103

[26] Braun A, Zimmer K, Hosselbarth B, Meinhardt J, Bigl F and Mehnert R 1998 Excimer laser micromachining and replication of 3D optical surfaces *Appl. Surf. Sci.* **127** 911–4

[27] Cheng Y, Tsai H L, Sugioka K and Midorikawa K 2006 Fabrication of 3D microoptical lenses in photosensitive glass using femtosecond laser micromachining *Appl. Phys.* A **85** 11–4

[28] Fleischer J, Halvadjiysky G and Haupt S 2008 Process parameter analysis in ablating micro-mold manufacturing *Microsyst. Technol.* **14** 1367–72
[29] Knowles M R H, Rutterford G, Karnakis D and Ferguson A 2007 Micro-machining of metals, ceramics and polymers using nanosecond lasers *Int. J. Adv. Manuf. Technol.* **33** 95–102
[30] Li J and Ananthasuresh G K 2001 A quality study on the excimer laser micromachining of electro-thermal-compliant micro devices *J. Micromech. Microeng.* **11** 38–47
[31] Pfleging W, Bernauer W, Hanemann T and Torge M 2002 Rapid fabrication of microcomponents—UV-laser assisted prototyping, laser micro-machining of mold inserts and replication via photomolding *Microsyst. Technol.* **9** 67–74
[32] Pfleging W, Hanemann T, Torge M and Bernauer W 2003 Rapid fabrication and replication of metal, ceramic and plastic mould inserts for application in microsystem technologies *Proc. Inst. Mech. Eng.* C **217** 53–63
[33] Shiu P P, Knopf G K, Ostojic M and Nikumb S 2008 Rapid fabrication of tooling for microfluidic devices via laser micromachining and hot embossing *J. Micromech. Microeng.* **18** 025012
[34] Smith C W, Herbert R, Wootton R J and Evans K E 2000 The hind wing of the desert locust (Schistocerca gregaria Forskal): II. Mechanical properties and functioning of the membrane *J. Exp. Biol.* **203** 2933–43
[35] Song F, Lee K L, Soh A K, Zhu F and Bai Y L 2004 Experimental studies of the material properties of the forewing of cicada (Homoptera, Cicadidae) *J. Exp. Biol.* **207** 3035–42
[36] Song F, Xiao K W, Bai K and Bai Y L 2007 Microstructure and nanomechanical properties of the wing membrane of dragonfly *Mater. Sci. Eng.* A **457** 254–60
[37] Vincent J F V and Wegst U G K 2004 Design and mechanical properties of insect cuticle *Arthropod Struct. Dev.* **33** 187–99
[38] Linder V, Gates B D, Ryan D, Parviz B A and Whitesides G M 2005 Water-soluble sacrificial layers for surface micromachining *Small* **1** 730–6
[39] Marks L S 1951 *Mechanical Engineers' Handbook* 5th edn (New York: McGraw-Hill)
[40] Ellington C P 1984 The aerodynamics of hovering insect flight: II. Morphological parameters *Phil. Trans. R. Soc.* B **305** 17–40
[41] Steppan S J 1996 Flexural stiffness patterns of butterfly wings (Papilionoidea) *J. Res. Lepid.* **35** 61–77